




# Heteronuclear Bimetallic Complexes with 3d and 4f Elements

Brian A. Chalmers , David B. Cordes , Lauren Bertram, Daniel J. Harraghy, Rachel C. Reid, Iain A. Smellie , Anna E. Tarcza and Brodie J. Thomson

EaStCHEM School of Chemistry, University of St Andrews, North Haugh, St Andrews, Fife KY16 9ST, UK

\* Correspondence: bac8@st-andrews.ac.uk; Tel.: +44-1334-463785

**Abstract:** Three heteronuclear bimetallic complexes [Cu(MeOH)(L)Ln(NO<sub>3</sub>)<sub>3</sub>] (**1-Ce**; Ln = Ce, **1-Pr**; Ln = Pr, and **1-Nd**; Ln = Nd) were prepared using H<sub>2</sub>L (1,3-bis[(3-methoxysalicylidene)amino]-2,2-dimethylpropane) in methanol, affording the complexes as green crystalline materials. These can be prepared in a one-pot synthesis from 2,2-dimethylpropan-1,3-diamine, *o*-vanillin, copper(II) nitrate, and Ln(III) nitrate (Ln = Ce, Pr, Nd). X-ray crystallography, high-resolution mass spectrometry, and UV-vis spectroscopy were used to characterize the bimetallic complexes. All three complexes showed the copper center adopting a five-coordinate square pyramidal geometry and the lanthanoid cation adopting a ten-coordinate geometry.

**Keywords:** X-ray crystallography; bimetallic complexes; UV-vis spectroscopy; HRMS spectrometry

## 1. Introduction

Heteronuclear complexes containing both 3d- and 4f-metal ions are of wide interest due to their probable magnetic, electronic, and luminescent properties [1–3], as well as their uses in metal-organic frameworks and polymers [4,5]. The hexadentate ligand 1,3-bis[(3-methoxysalicylidene)amino]-2,2-dimethylpropane (H<sub>2</sub>L) contains two distinct sites for metal coordination [6]: an internal site with four chelating centers (two N- and two O- donors) and an outer site with four O- donors. This versatile ligand has been reported in many coordination complexes, often as mononuclear or dinuclear complexes, and has shown use in catalysis [7–9]. As a result of the flexibility of the ligand, the outer coordination site can easily accommodate large f-block cations. Early work on complexes of L coordinated to both a 3d- and a 4f-metal was focused on gaining an understanding of the magnetic properties and behavior of 3d-4f complexes, [10–15] but that has been followed more recently by studies on their uses as single-molecule magnets [16–20] and photoluminescent [21] properties.

Herein, we report three bimetallic complexes of L, [Cu(MeOH)(L)Ln(NO<sub>3</sub>)<sub>3</sub>] (Ln = Ce, Pr, Nd). The sequential addition of copper(II) nitrate to H<sub>2</sub>L, followed by either cerium(III), praseodymium, or neodymium(III) nitrate affords high yields of **1-Ce**, **1-Pr**, and **1-Nd**, respectively. The slow evaporation of a methanolic solution of each complex leads to the formation of dark green crystals.

## 2. Results

### 2.1. Synthesis and Characterization

The hexadentate ligand H<sub>2</sub>L can be prepared in a good yield (89%) from the reaction of 2,2-dimethylpropan-1,3-diamine with *o*-vanillin in methanol at ambient conditions, according to the reported method [22] (Scheme 1). The ligand can be isolated and characterized, or the synthesis of **1-Ce**, **1-Pr**, and **1-Nd** can be completed in a “one-pot” method by the slow addition of a methanolic solution of copper(II) nitrate, followed by the addition of a methanolic solution of either cerium(III), praseodymium, or neodymium(III) nitrate around 20 min after the addition of the copper. The solids are isolated as green powders via filtration. Crystals suitable for single crystal X-ray diffraction are grown from the slow



**Citation:** Chalmers, B.A.; Cordes, D.B.; Bertram, L.; Harraghy, D.J.; Reid, R.C.; Smellie, I.A.; Tarcza, A.E.; Thomson, B.J. Heteronuclear Bimetallic Complexes with 3d and 4f Elements. *Molbank* **2023**, *2023*, M1577. <https://doi.org/10.3390/M1577>

Academic Editor: René T. Boeré

Received: 22 December 2022

Revised: 30 January 2023

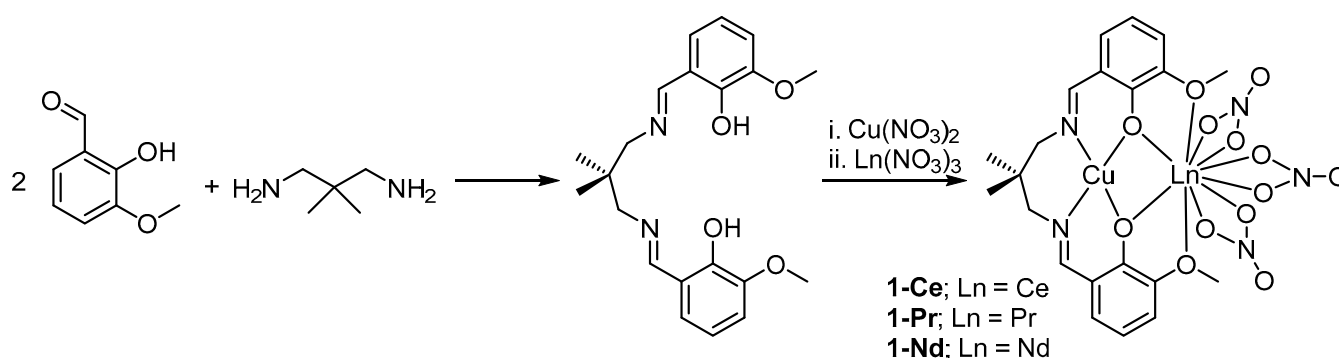
Accepted: 1 February 2023

Published: 3 February 2023



**Copyright:** © 2023 by the authors. Licensee MDPI, Basel, Switzerland. This article is an open access article distributed under the terms and conditions of the Creative Commons Attribution (CC BY) license (<https://creativecommons.org/licenses/by/4.0/>).

evaporation of a saturated solution of **1-Ce**, **1-Pr**, or **1-Nd** in methanol. The compounds are air- and moisture-stable as solids and show no signs of degradation or aerial oxidation after several months.



**Scheme 1.** Preparation of H<sub>2</sub>L and bimetallic complexes.

The solution state <sup>1</sup>H and <sup>13</sup>C DEPTQ NMR spectra of H<sub>2</sub>L confirm the identity of the ligand and match well with the known literature data [6,23]. The most deshielded environment is the phenolic proton at δ<sub>H</sub> 13.87 ppm, followed by the imine proton at δ<sub>H</sub> 8.53 ppm, with the most shielded environments being the two methyl groups on the propyl chain at δ<sub>H</sub> 0.99 ppm.

The infrared spectra of the bimetallic complexes (**1-Ce**, **1-Pr**, and **1-Nd**) confirm the inclusion of the nitrate ligands bonded to the lanthanoid ion, as they show the prominent wide bands at *ca.* 1520–1390 cm<sup>-1</sup> corresponding to ν(N=O) and ν<sub>as</sub>(NO<sub>2</sub>). The ν<sub>s</sub>(NO<sub>2</sub>) bands between 1060 and 1000 cm<sup>-1</sup> are characteristic of the nitrate ligand chelating in a bidentate mode [24,25]. The C=N stretching vibrations are also observed around 1630–1620 cm<sup>-1</sup> in H<sub>2</sub>L and all three bimetallic complexes. The overlay of the IR spectra of **1-Ce**, **1-Pr**, and **1-Nd** (Figure S9, see supporting information) shows there is very little difference between these complexes.

The UV-vis spectrum of H<sub>2</sub>L shows two strong bands at λ<sub>max</sub> 326 (π → π\*) and 419 (n → π\*) nm, with molar extinction coefficients (ε) of 3461 and 2917 mol dm<sup>-3</sup> cm<sup>-1</sup>, respectively [8]. The UV-vis spectra of **1-Ce**, **1-Pr**, and **1-Nd** are very similar with only minor differences in the λ<sub>max</sub> values of 629, 631, and 633 nm, respectively. These peaks also have very similar molar extinction coefficients (ε) of *ca.* 52–54 mol dm<sup>-1</sup> cm<sup>-1</sup>, corresponding to *d* → *d* transitions. In the spectrum of **1-Nd**, sharp bands at 525, 581, 736, 797, and 870 nm can be identified arising from the weak, Laporte-forbidden, *f*–*f* transitions, with the most intense of these being the <sup>4</sup>I<sub>9/2</sub> → <sup>4</sup>G<sub>5/2</sub> transition at 581 nm [26].

The high-resolution mass spectra of **1-Ce**, **1-Pr**, and **1-Nd** show the characteristic molecular ions expected. The HRMS shows peaks at *m/z* 694.9838, 695.9863, and 698.9879 corresponding to [CuCe(L)(NO<sub>3</sub>)<sub>2</sub>], [CuPr(L)(NO<sub>3</sub>)<sub>2</sub>], and [CuNd(L)(NO<sub>3</sub>)<sub>2</sub>] fragments, respectively. These show the isotope pattern expected from the inclusion of Ce, Pr, and Nd in these complexes.

## 2.2. X-ray Structures

Crystals of **1-Ce**, **1-Pr**, and **1-Nd** are grown by the slow evaporation of a saturated solution of the complex in methanol. The three structures show the copper(II) center adopts a five-coordinate square pyramidal geometry in the inner coordination site of L, with methanol taking up the axial coordination site. The lanthanoid ion (Ce(III) in **1-Ce**, Pr(III) in **1-Pr**, and Nd(III) in **1-Nd**) occupies the outer coordination site, adopting a ten-coordinate geometry, with four M–O bonds to the ligand, and six M–O bonds to the nitrate ligands (Figure 1). There are minor differences in the structure and packing of **1-Nd**; however, **1-Ce** and **1-Pr** are isostructural. Powder X-ray diffraction (PXRD) data are collected on the as-prepared samples of all three complexes at ambient temperature. A comparison of these PXRD patterns to those calculated from the single crystal structures (Figures S1 and S2)

confirms both the purity of the complexes, and that the structures in the bulk match those of the crystals.

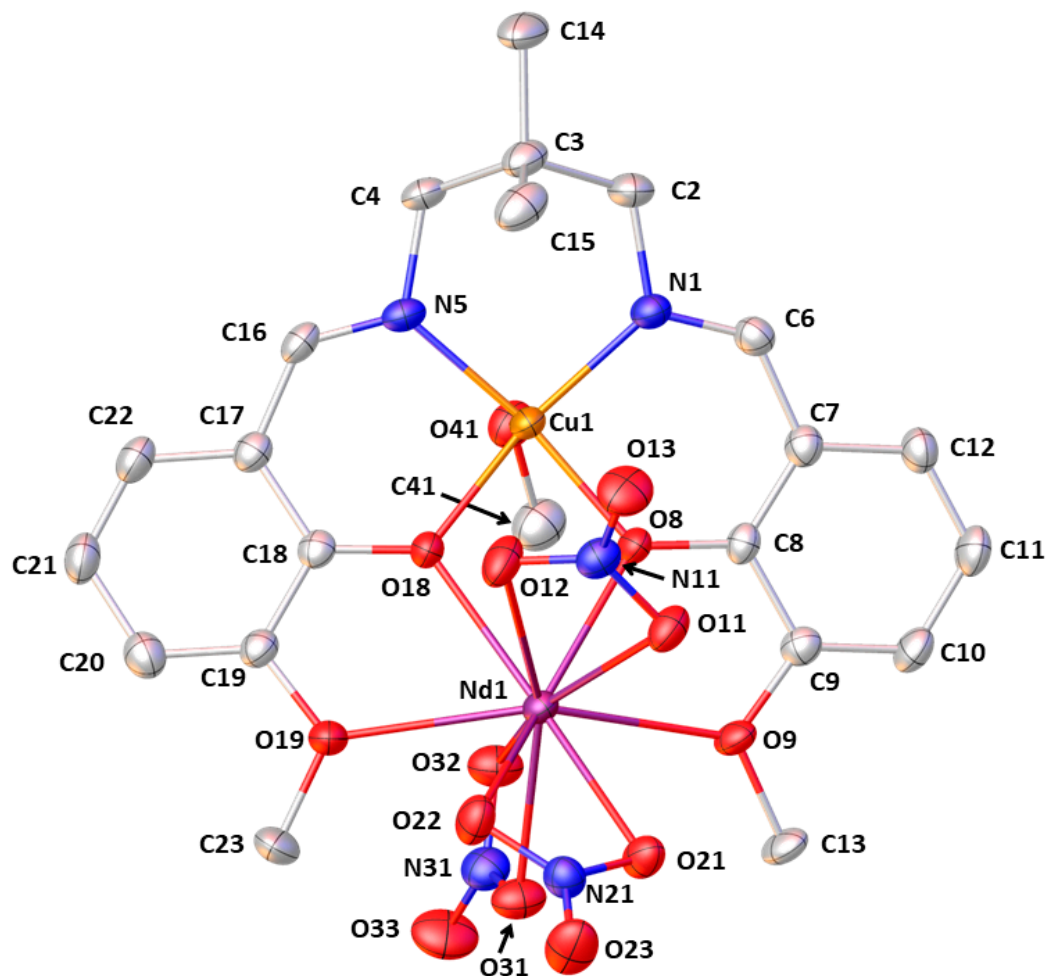


**Figure 1.** Molecular structure of **1-Nd**. Hydrogen atoms are omitted for clarity. Anisotropic displacement ellipsoids are set at the 50% probability level. Images of **1-Ce** and **1-Pr** can be seen in Figure S26.

In complex **1-Ce**, the copper is coordinated by two nitrogen and two phenolic oxygen donors (Table 1). The methanolic Cu1–O41 bond length is elongated relative to the other Cu–O bonds at 2.341(2) Å, typical of tetragonal distortions associated with copper(II) ions. The square pyramidal geometry is slightly distorted (Table 1) due to the constraints imposed by the ligand. The bond lengths and angles about copper show no significant changes between **1-Ce** and **1-Pr**. The Cu–N and Cu–O bond lengths do not change in **1-Nd** (Table 1), although a slightly wider range of angles is seen.

The Ln–O bonds to the phenolate oxygen atoms (O8/O18) are marginally shorter by around 0.12 Å than the bonds to the methoxy group (O9/O19) (Table 1). The cerium coordination sphere is completed by three  $\kappa^2$ -O-binding nitrate ligands with Ce–O bond lengths ranging from 2.5511(17) Å to 2.6371(18) Å. In **1-Pr** and **1-Nd**, there are no significant changes or deviations in bond lengths or angles when compared to **1-Ce**.

**Table 1.** Selected bond lengths (Å) and angles (degrees) for compounds **1-Ce**, **1-Pr**, and **1-Nd**.

	<b>1-Ce</b>	<b>1-Pr</b>	<b>1-Nd</b>
Cu1–N1	2.0020(19)	2.0039(17)	1.997(2)
Cu1–N5	1.9579(19)	1.9560(17)	1.974(2)
Cu1–O8	1.9534(15)	1.9536(14)	1.9589(17)
Cu1–O18	1.9689(15)	1.9634(14)	1.9639(18)
Cu1–O41	2.3400(17)	2.3404(15)	2.3436(19)
Ln1–O8	2.4313(15)	2.4155(14)	2.4113(18)
Ln1–O9	2.5912(16)	2.5789(14)	2.5391(17)
Ln1–O18	2.4663(15)	2.4520(14)	2.4468(17)
Ln1–O19	2.6243(16)	2.6122(14)	2.5766(19)
Cu1···Ln1	3.5896(4)	3.5747(4)	3.5758(6)
N1–Cu1–N5	96.02(8)	96.14(7)	96.68(9)
O8–Cu1–O18	80.00(6)	79.82(6)	78.67(7)
O8–Ln1–O18	61.96(5)	62.16(5)	61.57(6)
O9–Ln1–O19	148.10(5)	148.06(5)	149.70(6)

The distances between the copper and the lanthanoid atoms are very similar at 3.5896(4), 3.5747(4), and 3.5758(6) Å, for **1-Ce**, **1-Pr**, and **1-Nd**, respectively. This is just out with the sum of their van der Waals radii (3.4 Å for Cu···Ce, Cu···Pr, and Cu···Nd), meaning there is little interaction between the two elements [27].

In **1-Ce** and **1-Pr**, the ligand is slightly more distorted than in **1-Nd**, as shown by the angle between the mean planes of the phenyl rings increasing from 13.96(13)° in **1-Nd** to 27.87(13)° in **1-Ce** and 27.37(11)° in **1-Pr**. There are some significant differences in the long-range order between the two structure-types observed. The most significant of these is that the methanol ligand coordinates to the copper at a different orientation, changing the resulting hydrogen-bonding pattern. In **1-Ce** and **1-Pr**, the dominant hydrogen-bonding pattern is from the hydroxyl of the methanol to one of the nitrate ligands (O41–H41···O33A(-X, -Y, -Z+1)), forming centrosymmetric dimers with H···O 2.08 Å, and the corresponding O···O of 2.912(3) and 2.915(2) Å (Figure 2) for **1-Ce** and **1-Pr**, respectively.

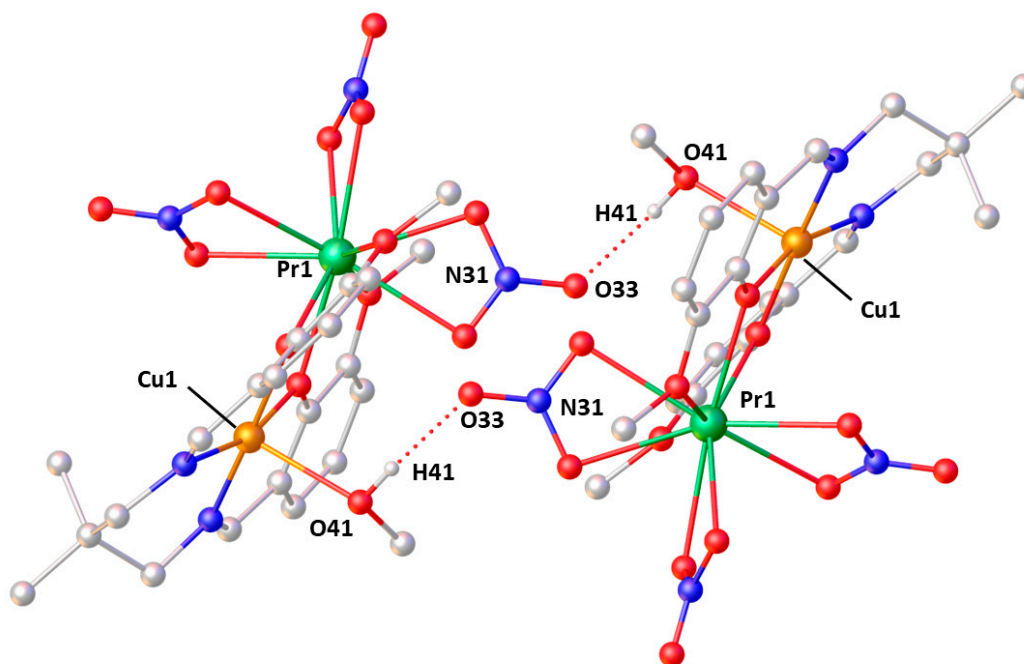


**Figure 2.** The dominant hydrogen-bonding interactions in **1-Pr**. The same interactions occur in **1-Ce**. All carbon-bound hydrogen atoms are omitted for clarity.

In contrast, in **1-Nd**, while hydrogen bonds again form between the methanol ligand and a nitrate ligand (O41–H41···O11A(X-1, Y, Z)), their relative orientations result in the formation of 1D chains running along the *a*-axis, with H···O of 2.09 Å and the corresponding O···O of 2.914(3) Å (Figure 3).

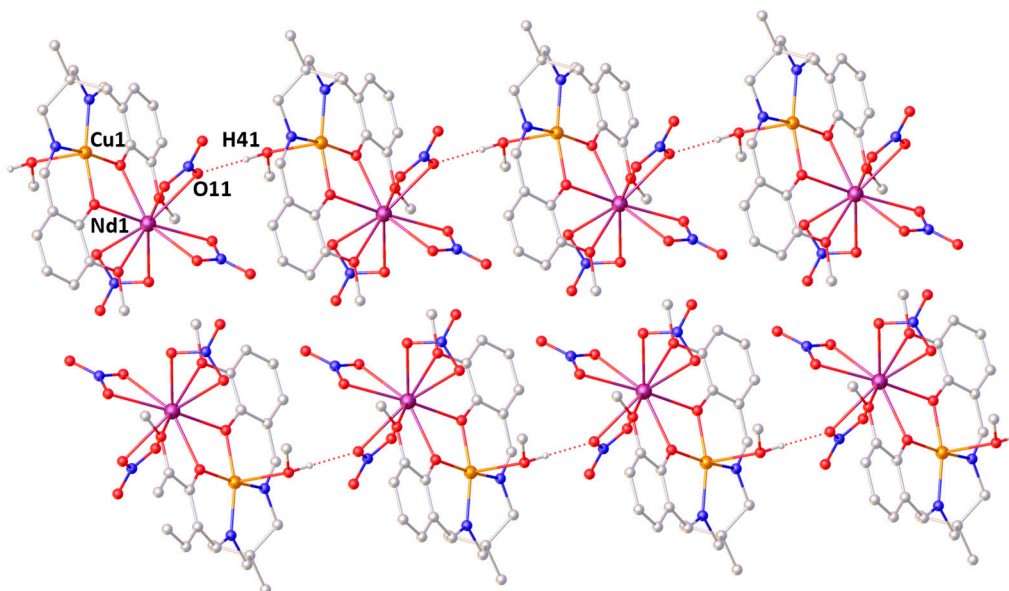


**Figure 3.** The dominant hydrogen-bonding interactions in **1-Nd** showing the 1D chains along the *a*-axis. All carbon-bound hydrogen atoms are omitted for clarity.

The packing in **1-Ce** also results in 1D chains along the *a*-axis; however, these arise from weak CH···O interactions between C16–H16···O13, in contrast to **1-Nd** (Figure S20). There are other weaker CH···O interactions in **1-Ce** resulting in the formation of different dimers in the crystal. One set occurs between C2–H2A···O41, another between C15–H15C···O12, and a final one between C20–H20···O23 (Figures S21–S23). Identical weak chain- and dimer-forming interactions can be seen in **1-Pr**. However, in **1-Nd**, due to the different orientation of the methanol ligand, all CH···O interactions form dimers. There are three sets of interactions, and two of these work cooperatively; C13–H13B and C41–H41B interact jointly with O33, while the other dimer-forming interaction is between C20–H20···O23 (Figures S24 and S25).

The packing is generally the same in **1-Ce**, **1-Pr**, and **1-Nd**; however, there is a different combined pattern of interactions resulting in **1-Ce/1-Pr** forming a 3D network, with **1-Nd** forming 2D interacting sheets in the *ab* plane with no significant interactions between them. This suggests that the dominant factor in the packing of these structures is the geometric arrangement of packing the molecules together, with different interactions arising from minor geometric changes, rather than a different set of interactions leading to differences in packing.

There are twenty complexes of the form  $[M_{3d}(\text{solvent})(L)M_{4f}(\text{NO}_3)_3]$  in the Cambridge Structural Database [28]. Of the six complexes where  $M_{3d}$  is Cu(II), the *f*-block metals present are Gd–Er, and the copper-coordinating solvents are either acetone or water [10,16,17]. There are also two complexes where the coordinating solvent is methanol, bound to Co(II) [14], or Fe(II) [13]. None of these complexes show an isostructural unit cell to those of **1-Ce**, **1-Pr**, and **1-Nd**, although many of them are isostructural with each other. Most of these complexes show the ligands in a relatively planar arrangement (angles between the phenyl ring mean planes of 2.99–10.76°), with the exception of the copper-aqua complex which has a less-planar ligand (angle between the phenyl ring mean planes 21.48°) [16], although it is not distorted to the extent seen in **1-Ce** and **1-Pr**. The dimethylpropane group of L takes the expected orientation in these complexes, with the methyl group on the face opposite the coordinated solvent molecule. The one exception to this is

the copper-aqua complex, which has them pointing to the same face as the coordinated water, and then forming a weak intramolecular CH $\cdots$ O interaction. The majority of these complexes do not show the same patterns of interactions as complexes **1-Ce**, **1-Pr**, and **1-Nd**. With no functionality to form conventional hydrogen bonds, the only interactions possible for the acetone complexes are weak CH $\cdots$ O interactions, which give rise to 3D networks. The copper-aqua complex forms both intra- and intermolecular hydrogen bonds, which give rise to one-dimensional chains running along the *b*-axis. These are linked into three dimensions via weak CH $\cdots$ O interactions. The Fe(II)-methanol complex shows a similar pattern of interactions to the copper-aqua complex; forming one-dimensional hydrogen-bonded chains along the *a*-axis, which are linked into a 3D network by weak CH $\cdots$ O interactions. However, many of these interactions are mediated by additional non-coordinated methanol solvent molecules. In contrast, the Co(II)-methanol complex shows hydrogen-bonded dimers similar to those seen in **1-Ce** and **1-Pr**; however, these are then linked into 2D sheets in the (1 0 -1) plane by weak CH $\cdots$ O interactions.

### 3. Materials and Methods

#### 3.1. General Considerations

All synthetic manipulations were performed in air. Each apparatus was dried in an oven (*ca.* 110 °C) prior to use. Solvents and chemicals were used as provided without further purification. IR spectra were recorded on a Perkin Elmer Spectrum Two instrument with DTGS detector and diamond ATR attachment. UV-vis spectra were acquired as solutions in methanol with a 1 cm path length in the range 850–300 nm using a Shimadzu spectrophotometer. The HRMS data were acquired from the University of St Andrews Mass Spectrometry Service. All NMR spectra were recorded using a Bruker Avance II 400 (MHz) spectrometer at 20 °C. Assignments of  $^1\text{H}$  and  $^{13}\text{C}$  NMR spectra were made in conjunction with the appropriate two-dimensional experiments. The  $^{13}\text{C}$  NMR spectrum was recorded using the DEPTQ-135 pulse sequence with broadband proton decoupling. Tetramethylsilane was used as an external standard ( $\delta_{\text{H}}$ ,  $\delta_{\text{C}}$  0.00 ppm). Chemical shifts ( $\delta$ ) are given in parts per million (ppm) relative to the solvent peaks. Coupling constants (*J*) are given in Hertz (Hz). Spectra were analyzed using the MestReNova software package.

#### 3.2. Syntheses

##### 3.2.1. Synthesis of H<sub>2</sub>L

This was prepared using an adapted version of the literature method [22]. A solution of *o*-vanillin (2.00 g, 13.2 mmol) in methanol (20 mL) was prepared. To this, a solution of 2,2-dimethylpropan-1,3-diamine (0.68 g, 6.6 mmol) in methanol (10 mL) was added dropwise, with continuous stirring over 10 min, forming a bright yellow solution. After 30 min, the volatiles were removed under reduced pressure and the oily liquid left to stand for 24 h. After this time, solid H<sub>2</sub>L was isolated as a yellow powder (2.34 g 97%).

The NMR numbering scheme is provided in Figure 4.  $^1\text{H}$  NMR (400.3 MHz, *d*<sub>6</sub>-DMSO)  $\delta_{\text{H}}$  13.87 (2H, s, H-12), 8.53 (2H, s, H-4), 7.06–7.01 (4H, m, H-8,10), 6.81 (2H, t,  $^3J_{\text{HH}}$  7.9 Hz, H-9), 3.78 (6H, s, H-11), 3.49 (4H, s, H-3), 0.99 (6H, s, H-1).  $^{13}\text{C}$  DEPTQ (100.6 MHz, *d*<sub>6</sub>-DMSO)  $\delta_{\text{C}}$  167.3 (s, C-4), 152.2 (s, qC-6), 148.5 (s, qC-7), 123.6 (s, C-10), 118.7 (s, qC-5), 118.2 (s, C-9), 115.2 (s, C-8), 67.1 (s, C-3), 36.2 (s, qC-2), 24.1 (s, C-1). IR:  $\nu_{\text{max}}$  (ATR/ $\text{cm}^{-1}$ ) 3008w ( $\nu_{\text{C-H}}$ ), 2959w ( $\nu_{\text{C-H}}$ ), 2838w ( $\nu_{\text{C-H}}$ ), 1628s ( $\nu_{\text{C=N}}$ ), 1470s, 1394m, 1339m, 1248vs ( $\nu_{\text{C-O}}$ ), 1168m ( $\nu_{\text{C-O}}$ ), 1078s, 1038s, 974m, 872m, 783s, 741s, 727s, 637m. UV-vis:  $\lambda_{\text{max}}$  (MeOH)/nm ( $\epsilon$   $\text{dm}^3 \text{mol}^{-1} \text{cm}^{-1}$ ) 326 (3461,  $\pi \rightarrow \pi^*$ ), 419 (2917,  $n \rightarrow \pi^*$ ).

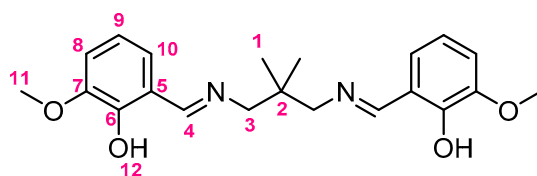


Figure 4. NMR numbering scheme for H<sub>2</sub>L.

### 3.2.2. One-Pot Synthesis of **1-Ce**, **1-Pr**, and **1-Nd**

A solution of *o*-vanillin (1.00 g, 6.6 mmol) in methanol (10 mL) was prepared. To this, a solution of 2,2-dimethylpropan-1,3-diamine (0.34 g, 3.3 mmol) in methanol (5 mL) was added dropwise, with continuous stirring, over 10 min. Separately, solutions of copper(II) nitrate trihydrate (0.80 g, 3.3 mmol), cerium(III) nitrate hexahydrate (1.95 g, 4.4 mmol) (for **1-Ce**), praseodymium(III) nitrate hexahydrate (1.95 g, 4.4 mmol) (for **1-Pr**), or neodymium(III) nitrate hexahydrate (1.96 g, 4.4 mmol) (for **1-Nd**), were prepared.

After the bright yellow H<sub>2</sub>L solution had been stirred for 30 min, the blue copper solution was added dropwise over 10 min, giving a dark green solution. This was allowed to stir for a further 20 min before either the cerium, praseodymium, or neodymium solution was added dropwise over 15 min. After stirring for 1 h, the solution was filtered under a vacuum to afford **1-Ce**, **1-Pr**, or **1-Nd** as a green powder (**1-Ce**: 1.76 g, 67%; **1-Pr**: 1.59 g, 61%; **1-Nd**: 1.96 g, 75%).

### 3.2.3. Analytical Data for **1-Ce**

HRMS (ES<sup>+</sup>): *m/z* (%) Calcd. for C<sub>21</sub>H<sub>24</sub>N<sub>4</sub>O<sub>10</sub>CuCe: 694.9843, found: 694.9838 [M–NO<sub>3</sub>–MeOH] (100). IR:  $\nu_{\max}$  (ATR/cm<sup>−1</sup>) 3464w, 2954w ( $\nu_{\text{C-H}}$ ), 1623m ( $\nu_{\text{C=N}}$ ), 1466s ( $\nu_{\text{N=O}}$ ,  $\nu_{\text{NO}_2}$ ), 1292s, 1230s, 1102w, 1063m ( $\nu_{\text{NO}_2}$ ), 1003m, 973m, 933m, 853m, 816m, 778w, 733s, 646m, 619m. UV-vis:  $\lambda_{\max}$  (MeOH)/nm ( $\epsilon$  dm<sup>3</sup> mol<sup>−1</sup> cm<sup>−1</sup>) 629 (52).

### 3.2.4. Analytical Data for **1-Pr**

HRMS (ES<sup>+</sup>): *m/z* (%) Calcd. for C<sub>21</sub>H<sub>24</sub>N<sub>4</sub>O<sub>10</sub>CuPr: 695.9865, found: 695.9863 [M–NO<sub>3</sub>–MeOH] (100). IR:  $\nu_{\max}$  (ATR/cm<sup>−1</sup>) 3469w, 2955w ( $\nu_{\text{C-H}}$ ), 1623m ( $\nu_{\text{C=N}}$ ), 1467s ( $\nu_{\text{N=O}}$ ,  $\nu_{\text{NO}_2}$ ), 1293s, 1229s, 1102w, 1064m ( $\nu_{\text{NO}_2}$ ), 1000m, 973m, 934m, 853m, 816m, 778w, 734s, 646m, 619m. UV-vis:  $\lambda_{\max}$  (MeOH)/nm ( $\epsilon$  dm<sup>3</sup> mol<sup>−1</sup> cm<sup>−1</sup>) 631 (54).

### 3.2.5. Analytical Data for **1-Nd**

HRMS (ES<sup>+</sup>): *m/z* (%) Calcd. for C<sub>21</sub>H<sub>24</sub>N<sub>4</sub>O<sub>10</sub>CuNd: 698.9866, found: 698.9879 [M–NO<sub>3</sub>–MeOH] (100). IR:  $\nu_{\max}$  (ATR/cm<sup>−1</sup>) 3464w, 2954w ( $\nu_{\text{C-H}}$ ), 1623m ( $\nu_{\text{C=N}}$ ), 1466s ( $\nu_{\text{N=O}}$ ,  $\nu_{\text{NO}_2}$ ), 1292s, 1230s, 1102w, 1063m ( $\nu_{\text{NO}_2}$ ), 1003m, 973m, 933m, 853m, 816m, 778w, 733s, 646m, 619m. UV-vis:  $\lambda_{\max}$  (MeOH)/nm ( $\epsilon$  dm<sup>3</sup> mol<sup>−1</sup> cm<sup>−1</sup>) 633 (53).

### 3.2.6. Crystallographic Details

Ambient temperature powder X-ray diffraction (PXRD) data were collected on a PANalytical Empyrean Diffractometer in Bragg-Brentano geometry using Cu K $\alpha$ <sub>1</sub> radiation ( $\lambda = 1.54060$  Å). Data were collected in the range of 5° to 70°, with a step size of 0.017°, and a time per step of 0.94 s.

Green X-ray quality crystals of **1-Ce**, **1-Pr**, and **1-Nd** were grown from the slow evaporation of a saturated solution of the complex in methanol at ambient conditions. X-ray diffraction data for all three compounds were collected at 173 K using a Rigaku FR-X Ultrahigh Brilliance Microfocus RA generator/confocal optics with XtaLAB P200 diffractometer [Mo K $\alpha$  radiation ( $\lambda = 0.71075$  Å)]. Intensity data were collected using  $\omega$  steps accumulating area detector images spanning at least a hemisphere of reciprocal space. Data for all compounds analyzed were collected and processed (including correction for Lorentz, polarization, and absorption) using CrystalClear [29]. Structures were solved by Patterson methods (PATTY [30]) and refined by full-matrix least-squares against F<sup>2</sup>

(SHELXL-2018/3) [31]. Non-hydrogen atoms were refined anisotropically, and hydrogen atoms were refined using a riding model. All calculations were performed using the CrystalStructure interface [32]. Selected crystallographic data are presented in Table S1. CCDC 2224393–2224395 contain the supplementary crystallographic data for this paper. These data can be obtained free of charge from The Cambridge Crystallographic Data Centre via [www.ccdc.cam.ac.uk/structures](http://www.ccdc.cam.ac.uk/structures).

#### 4. Conclusions

The tetradentate ligand H<sub>2</sub>L has been used to prepare three novel complexes containing both a 3d- and 4f-metal (3d = Cu, 4f = Ce, Pr, Nd). The complexes were characterized by single-crystal X-ray diffraction, UV-vis spectrophotometry, mass spectrometry, and IR spectroscopy. The copper center adopted a square pyramidal geometry with one molecule of methanol coordinating. The lanthanoid element adopted a 10-coordinate geometry with four M–O bonds to H<sub>2</sub>L, and six M–O bonds to the nitrate ligands.

**Supplementary Materials:** The following supporting information can be downloaded online. Figures S1–S2: PXRD patterns of **1-Ce**, **1-Pr**, **1-Nd**; Figure S3: <sup>1</sup>H NMR spectrum of H<sub>2</sub>L; Figure S4: <sup>13</sup>C DEPTQ NMR spectrum of H<sub>2</sub>L; Figures S5–S9: IR spectra of reported compounds; Figures S10–S15: HRMS spectra of bimetallic complexes; Figures S16–S19: UV-vis spectra of reported compounds; Figures S20–S26: Additional interactions in the solid-state; Table S1: Selected crystallographic data; Video S1: Structures 360° rotation movie; CIF files of **1-Ce**, **1-Pr**, and **1-Nd**.

**Author Contributions:** This work has been conducted as part of a research project involving undergraduate students (L.B., D.J.H., R.C.R., A.E.T. and B.J.T.); all the required synthetic steps and preliminary analysis were carried out by this group. D.B.C. collected the X-ray data and solved the structures and contributed to writing the manuscript. B.A.C. and I.A.S. collected and carried out the analysis of the other spectroscopic data. B.A.C. designed the study, analyzed the data, and wrote the paper. All authors have read and agreed to the published version of the manuscript.

**Funding:** This research received no external funding.

**Data Availability Statement:** CCDC 2224393–2224395 contains the supplementary crystallographic data for this paper. These data can be obtained free of charge from The Cambridge Crystallographic Data Centre via [www.ccdc.cam.ac.uk/structures](http://www.ccdc.cam.ac.uk/structures).

**Acknowledgments:** This work was conducted as part of an undergraduate group research project at the University of St. Andrews. The authors express gratitude to the University of St. Andrews School of Chemistry for the use of their laboratory facilities and provision of materials with particular thanks to Yuri Andreev and Julia L. Payne for assistance with the PXRD data.

**Conflicts of Interest:** The authors declare no conflict of interest.

#### References

1. Winpenny, R.E.P. The structures and magnetic properties of complexes containing 3d- and 4f-metals. *Chem. Soc. Rev.* **1998**, *27*, 447–452. [[CrossRef](#)]
2. Piguet, C.; Bunzli, J.-C.G. Mono- and polymetallic lanthanide-containing functional assemblies: A field between tradition and novelty. *Chem. Soc. Rev.* **1999**, *28*, 347–358. [[CrossRef](#)]
3. Sakamoto, M.; Manseki, K.; Okawa, H. d-f Heteronuclear complexes: Synthesis, structures and physicochemical aspects. *Coord. Chem. Rev.* **2001**, *219–221*, 379–414. [[CrossRef](#)]
4. Abdelbaky, M.S.M.; Amghouz, Z.; Garcia-Granda, S.; Garcia, J.R. Synthesis, Structures and Luminescence Properties of Metal-Organic Frameworks Based on Lithium-Lanthanide and Terephthalate. *Polymers* **2016**, *8*, 86. [[CrossRef](#)] [[PubMed](#)]
5. Abdelbaky, M.S.M.; Amghouz, Z.; García-Granda, S.; García, J.R. A metal-organic framework assembled from Y(III), Li(I), and terephthalate: Hydrothermal synthesis, crystal structure, thermal decomposition and topological studies. *Dalton Trans.* **2014**, *43*, 5739–5746. [[CrossRef](#)]
6. Aguiari, A.; Bullita, E.; Casellato, U.; Guerriero, P.; Tamburini, S.; Vigato, P.A.; Russo, U. Preparation, properties and coordination behaviour of planar or tridimensional compartmental Schiff bases. *Inorg. Chim. Acta.* **1994**, *1–2*, 135–146. [[CrossRef](#)]
7. Thevenon, A.; Garden, J.A.; White, A.J.P.; Williams, C.K. Dinuclear Zinc Salen Catalysts for the Ring Opening Copolymerisation of Epoxides and Carbon Dioxide or Anhydrides. *Inorg. Chem.* **2015**, *54*, 11906–11915. [[CrossRef](#)]



8. Rayati, S.; Zakavi, S.; Koliaei, M.; Wojtczak, A.; Kozakiewicz, A. Electron-rich salen-type Schiff based complexes of Cu(II) as catalysts for oxidation of cyclooctene and styrene with *tert*-butylhydroperoxide: A comparison with electron-deficient ones. *Inorg. Chem. Commun.* **2010**, *13*, 203–207. [[CrossRef](#)]
9. Diment, W.T.; Stöber, T.; Kerr, R.W.F.; Phanopoulos, A.; Durr, C.B.; Williams, C.K. *Ortho*-vanillin derived Al(III) and Co(III) catalyst systems for switchable catalysis using  $\epsilon$ -decalactone phthalic anhydride and cyclohexene oxide. *Catal. Sci. Technol.* **2021**, *11*, 1737–1745. [[CrossRef](#)]
10. Costes, J.-P.; Dahan, F.; Dupuis, A.; Laurent, J.-P. A General Route to Strictly Dinuclear Cu(II)/Ln(III) Complexes. *Structural Determination and Magnetic Behavior of Two Cu(II)/Gd(III) Complexes*. *Inorg. Chem.* **1997**, *36*, 3429–3433. [[CrossRef](#)]
11. Costes, J.-P.; Dahan, F.; Dupuis, A.; Laurent, J.-P. Experimental Evidence of a Ferromagnetic Ground State ( $S = 9/2$ ) for a Dinuclear Gd(III)-Ni(II) Complex. *Inorg. Chem.* **1997**, *36*, 4284–4286. [[CrossRef](#)]
12. Costes, J.-P.; Dahan, F.; Donnadiou, B.; Garcia-Tojal, J.; Laurent, J.P. Versatility of the Nature of the Magnetic Gadolinium(III)-Vanadium(IV) Interaction—Structure and Magnetic Properties of Two Heterobinuclear [Gd, V(O)] Complexes. *Eur. J. Inorg. Chem.* **2001**, *2001*, 363–365. [[CrossRef](#)]
13. Costes, J.-P.; Clemente-Juan, J.M.; Dahan, F.; Dumestre, F.; Tuchagues, J.-P. Dinuclear (FeII, GdIII) Complexes Deriving from Hexadentate Schiff Bases: Synthesis, Structure, and Mössbauer and Magnetic Properties. *Inorg. Chem.* **2002**, *41*, 2886–2891. [[CrossRef](#)] [[PubMed](#)]
14. Costes, J.-P.; Dahan, F.; Garcia-Tojal, J. Dinuclear CoII/GdIII and CoIII/GdIII Complexes Derived from Hexadentate Schiff Bases: Synthesis, Structure, and Magnetic Properties. *Chem. Eur. J.* **2002**, *8*, 5430–5434. [[CrossRef](#)]
15. Cimpoesu, F.; Dahan, F.; Ladeira, S.; Ferbinteanu, M.; Costes, J.-P. Chiral Crystallization of a Heterodinuclear Ni-Ln Series: Comprehensive Analysis of the Magnetic Properties. *Inorg. Chem.* **2012**, *51*, 11279–11293. [[CrossRef](#)]
16. Kajiwara, T.; Takahashi, K.; Hiraizumi, T.; Takaishi, S.; Yamashita, M. Coordination enhancement of single-molecule magnet behaviour of Tb(III)–Cu(II) dinuclear systems. *Polyhedron* **2009**, *28*, 1860–1863. [[CrossRef](#)]
17. Ishida, T.; Watanabe, R.; Fujiwara, K.; Okazawa, A.; Kojima, N.; Tanaka, G.; Yoshii, S.; Nojiri, H. Exchange coupling in TbCu and DyCu single-molecule magnets and related lanthanide and vanadium analogs. *Dalton Trans.* **2012**, *41*, 13609–13619. [[CrossRef](#)]
18. Marius, A.; Costes, J.-P.; Diaz, C.; Gao, S. 3d-4f Combined Chemistry: Synthetic Strategies and Magnetic Properties. *Inorg. Chem.* **2009**, *48*, 3342–3359. [[CrossRef](#)]
19. Liu, K.; Shi, W.; Cheng, P. Towards heterometallic single-molecule magnets; Synthetic strategy, structures and properties of 3d-4f discrete complexes. *Coord. Chem. Rev.* **2015**, *289–290*, 74–122. [[CrossRef](#)]
20. Dey, A.; Acharya, J.; Chandrasekhar, V. Heterometallic 3d-4f Complexes as Single-Molecule Magnets. *Chem. Asian. J.* **2019**, *14*, 4433–4453. [[CrossRef](#)]
21. Pasatoiu, T.D.; Madalan, A.M.; Zamfirescu, M.; Tiseanu, C.; Andruh, M. One- and two-photon induced emission in heterobimetallic ZnII–SmIII and ZnII–TbIII complexes with a side-off compartmental ligand. *Phys. Chem. Chem. Phys.* **2012**, *14*, 11448–11456. [[CrossRef](#)] [[PubMed](#)]
22. Arnáiz, F.J.; Costes, J.-P.; García-Tojal, J. *Inorganic Experiments*, 3rd ed; Woollins, J.D., Ed.; Wiley-VCH verlag GmbH & Co, KGaA: Weinheim, Germany, 2010; pp. 283–286.
23. Costes, J.-P.; Laussac, J.-P.; Nicodème, F. Complexation of a Schiff baseligand having two coordination sites ( $N_2O_2$ ) and  $O_2O_2$ ) with lanthanide ions (Ln = La, Pr): An NMR study. *J. Chem. Soc. Dalton. Trans* **2002**, 2731–2736. [[CrossRef](#)]
24. Gaye, M.; Tamboura, F.B.; Sall, A.S. Spectroscopic Studies of Some Lanthanide(III) Nitrate Complexes Synthesised From A New Ligand 2,6-Bis(salicylaldehydehydrazone)-4-chlorophenol. *Bull. Chem. Soc. Ethiop.* **2003**, *17*, 27–34. [[CrossRef](#)]
25. Ferraro, J.R. The nitrate symmetry in metallic nitrates. *J. Mol. Spectra* **1960**, *4*, 99–105. [[CrossRef](#)]
26. Adiyodi, A.K.; Jyothy, P.V.; Unnikrishnan, N.V. UV-Vis Absorption and NIR-Stimulated Emission of  $Nd^{3+}$ : PVA Films. *J. Appl. Polym. Sci.* **2009**, *113*, 887–895. [[CrossRef](#)]
27. Bondi, A. Van der Waals Volumes and Radii. *J. Phys. Chem.* **1964**, *68*, 441–452. [[CrossRef](#)]
28. Groom, C.R.; Bruno, I.J.; Lightfoot, M.P.; Ward, S.C. The Cambridge Structural Database. *Acta Crystallogr. Sect. B Struct. Sci. Cryst. Eng. Mater.* **2016**, *72*, 171–179. [[CrossRef](#)]
29. *CrystalClear-SM Expert v2.1*; Rigaku Americas: The Woodlands, TX, USA; Rigaku Corporation: Tokyo, Japan, 2015.
30. Beurskens, P.T.; Beurskens, G.; de Gelder, R.; Garcia-Granda, S.; Gould, R.O.; Israel, R.; Smits, J.M.M. DIRDIF-99. Crystallography Laboratory, University of Nijmegen: Nijmegen, The Netherlands, 1999.
31. Sheldrick, G.M. Crystal structure refinement with SHELXL. *Acta Crystallogr. Sect. C Struct. Chem.* **2015**, *71*, 3–8. [[CrossRef](#)]
32. *CrystalStructure v4.3.0*; Rigaku Americas: The Woodlands, TX, USA; Rigaku Corporation: Tokyo, Japan, 2018.

**Disclaimer/Publisher’s Note:** The statements, opinions and data contained in all publications are solely those of the individual author(s) and contributor(s) and not of MDPI and/or the editor(s). MDPI and/or the editor(s) disclaim responsibility for any injury to people or property resulting from any ideas, methods, instructions or products referred to in the content.